Letter

Magnon-exciton proximity coupling at a van der Waals heterointerface

A. Gloppe,[1,2,*] M. Onga,[3] R. Hisatomi,[2] A. Imamoğlu,[4] Y. Nakamura,[2,5] Y. Iwasa,[3,6,†] and K. Usami[2,‡]

[1]*Université de Strasbourg, CNRS, Institut de Physique et Chimie des Matériaux de Strasbourg (IPCMS), UMR 7504, F-67000 Strasbourg, France*

[2]*Research Center for Advanced Science and Technology (RCAST), The University of Tokyo, Meguro-ku, Tokyo 153-8904, Japan*

[3]*Quantum-Phase Electronics Center (QPEC) and Department of Applied Physics, The University of Tokyo, Tokyo 113-8656, Japan*

[4]*Institute for Quantum Electronics, ETH Zurich, CH-8093 Zurich, Switzerland*

[5]*RIKEN Center for Quantum Computing (RQC), Wako, Saitama 351-0198, Japan*

[6]*RIKEN Center for Emergent Matter Science (CEMS), Wako, Saitama 351-0198, Japan*

(Received 23 September 2021; revised 27 January 2022; accepted 1 February 2022; published 7 March 2022)

We report on an optically probed ferromagnetic resonance experiment which elucidates the magnon-exciton coupling at the interface between a magnetic thin film and an atomically thin semiconductor. Our approach allies the long-lived magnons hosted in a film of yttrium iron garnet (YIG) to strongly bound excitons in a flake of a transition metal dichalcogenide, $MoSe_2$. The magnons induce on the excitons a dynamical valley Zeeman effect ruled by interfacial exchange interactions. This nascent class of hybrid system suggests new opportunities for information transduction between microwave and optical regions.

DOI: 10.1103/PhysRevB.105.L121403

The emergence of 2D materials, such as graphene, sheds a new light on condensed-matter physics, as these materials can be artificially stacked to combine, protect, or enhance individual pristine physical properties [1]. Atomically thin semiconducting transition metal dichalcogenides (TMDs), exhibiting a number of unique optical features such as large excitonic binding energies, and valley-contrasting exciton selection rules [2–4], attract a lot of attention as a new platform for quantum optics and nanophotonics [5–7]. By a static valley Zeeman effect, their exciton resonances are shifted by external magnetic fields [8–10] or by the interfacial exchange fields with a magnetic substrate [11–14].

In this work we study a heterostructure consisting of $MoSe_2$ flakes transferred onto a magnetic film made of yttrium iron garnet [Fig. 1(a)]. The film supports long-lived magnons, or magnetization oscillations [15] that can be coherently driven by microwaves. Magnons play a major role in spintronics circuits as a low-loss information carrier [16,17], and in quantum hybrid systems as a macroscopic quantum interface to superconducting quantum bits [18–20]. Realizing an interfacial coupling [21] between magnons and excitons, in contrast to previous efforts involving bulk magnets [22,23] or dilute ferromagnetic semiconductors [24,25], offers a promising way forward to connect these technologies to optics. Here we demonstrate this magnon-exciton coupling at a van der Waals heterointerface.

Figure 1(b) depicts schematically our experimental setup at room temperature. The heterostructure $MoSe_2$/YIG is placed in the gap of an electromagnet to saturate the YIG magnetization within the film plane ($H_{DC} \sim 0.1$ T/μ_0). Magnons in the uniform magnetostatic mode of the film are excited with a microwave loop antenna connected to a network analyzer. A typical spectrum of the microwave reflected off the antenna reveals the ferromagnetic resonance (FMR) in Fig. 2(b), centered at $\omega_m/2\pi = 5.64$ GHz with a

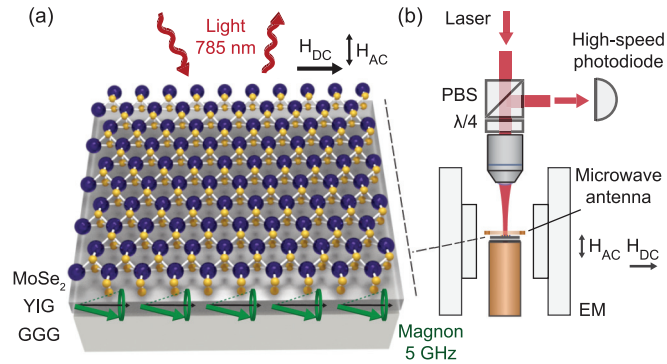

FIG. 1. Optically addressed TMD flake on a magnetic substrate supporting magnon modes. (a) Atomically thin flakes of $MoSe_2$ are stacked on a magnetic YIG film grown on gadolinium gallium garnet (GGG) [26]. The magnetization of the film is saturated by a static magnetic field H_{DC} directed within its plane. A microwave antenna excites magnons of the fundamental magnetostatic mode of frequency $\omega_m/2\pi \sim 5$ GHz through the alternating magnetic field H_{AC}. (b) The flakes are addressed normally with a focused laser beam at $\lambda_L = 785$ nm with a left- or right-handed circular polarization. A high-speed photodetector detects the optical signal reflected off the sample with the same polarization as input (EM: electromagnet, PBS: polarizing beamsplitter, λ/4: quarter-wave plate) [26].

*arnaud.gloppe@ipcms.unistra.fr
†iwasa@ap.t.u-tokyo.ac.jp
‡usami@qc.rcast.u-tokyo.ac.jp

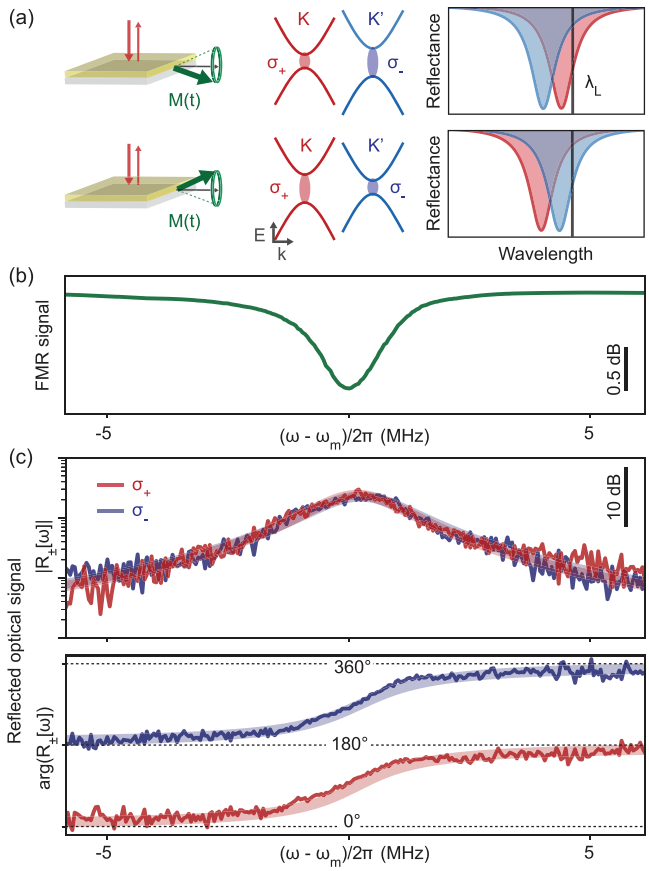

FIG. 2. Dynamical valley Zeeman effect. (a) Magnons support a coherent oscillation of the magnetization vector $M(t)$, responsible for an effective magnetic field modulating the excitonic resonances of the TMD flake through a dynamical valley Zeeman effect. Carrying opposite magnetic moments, the two valleys K and K' have their excitonic resonance shifting opposite ways when experiencing an out-of-plane magnetic field (E: relative energy, k: electron momentum). The reflectance of the flake at a fixed laser wavelength λ_L, on the edge of the excitonic resonance, is subsequently modulated at the magnon frequency. The phase of the reflected signal depends on the valley index, selectively addressed with left-handed σ_+ and right-handed σ_- circularly polarized light for K and K' valleys, respectively. (b) Microwave absorption signal revealing the ferromagnetic resonance (FMR) at $\omega_m/2\pi = 5.64\,\mathrm{GHz}$. (c) Magnitude and relative phase of the optically probed FMR spectra $R_\pm[\omega]$ on a $MoSe_2$ flake. The spectrum with the left (right)-handed circularly polarized light is plotted as a solid red (blue) line, superimposed on a red (blue) translucent Lorentzian fit (flake thickness: 20 nm, $n_{\mathrm{magnon}} = 10^{14}$, detection bandwidth: 5 Hz).

linewidth $\gamma_m/2\pi = 1.75\,\mathrm{MHz}$. With a continuous-wave laser ($\lambda_L = 785$ nm) we examine the light reflected from the heterostructure on a high-speed photodiode.

By analogy to valley Zeeman effects observed in TMDs with a static magnetic field [8–12], we expect the out-of-plane magnetization oscillations due to driven magnons to shift dynamically the excitonic resonance. The transverse magnetization per single magnon depends on the magnetic film volume, as our magnetostatic mode is delocalized over the entire magnetic film [26]. The relevant interaction Hamiltonian can be written as

$$H = \tau\,\hbar g\left(\frac{\hat{a}+\hat{a}^\dagger}{2}\right)\hat{x}^\dagger\hat{x}, \tag{1}$$

where $\tau = \pm 1$ is the index for K and K' valleys, and $\hat{a}$ ($\hat{a}^\dagger$) and $\hat{x}$ ($\hat{x}^\dagger$) are the annihilation (creation) operators for magnon and exciton, respectively [26]. The magnon-exciton coupling rate g corresponds to the excitonic resonance shift induced by a single magnon. This could stem from a short-range interfacial exchange field or from a long-range dipolar field. The microscopic origin of the coupling will be discussed later.

The choice of $MoSe_2$ is motivated by its bright excitons, with a high emission yield and a fundamental resonance around 800 nm [27] corresponding to a low-absorption window for YIG. In the absence of external magnetic field, photoluminescence measurements [26] show that the excitonic resonances of the $MoSe_2$ flakes are not significantly affected by their stacking on the YIG and match the typical values obtained on Si/SiO_2 substrates [27]. The optical reflectance of the flake at a fixed wavelength, situated on the edge of the excitonic resonance, should be subsequently modulated at the frequency of the magnetization oscillations [Fig. 2(a)], constituting a signature of the dynamical valley Zeeman effect. The tenuous Zeeman shift induced by the magnons at microwave frequencies would be otherwise challenging to observe with conventional optical spectroscopy methods.

We demonstrate that, through the dynamical valley Zeeman effect, the FMR can be optically probed by the focused laser beam illuminating the heterostructure at normal incidence. The left-handed (σ_+) and right-handed (σ_-) circularly polarized light mainly address the excitons in K and K' valleys, respectively. The reflected photons with the same helicity are detected on the high-speed photodiode. Inherited by the long magnon lifetime in YIG, the quality factor of the ferromagnetic resonance ($Q \sim 10^4$) enhances the magnon-induced Zeeman shift and the resulting optical signal. Figure 2(c) presents the reflected optical intensity around the FMR frequency $R_+[\omega]$ and $R_-[\omega]$, acquired with σ_+ and σ_- optical polarizations, respectively, picturing optically detected FMR spectra of a multilayer $MoSe_2$ flake (for a trilayer response, see [26]). The amplitudes $|R_\pm[\omega_m]|$ for both optical polarization, addressing K and K' valleys, are the same. Nevertheless, the two signals are phase shifted by π ($R_+[\omega_m] = -R_-[\omega_m]$). In TMD monolayers, the excitonic resonance shifts due to an out-of-plane magnetization are opposite for the two valleys K and K' [14,28]. Through this valley-resolved magnon-exciton coupling, the information of the microwave imprinted on the magnons is transferred to the reflected visible light via the excitons. It seems that the valley-contrasting features, which are characteristic of monolayers, are preserved even in multilayer flakes. However, as we discuss later and in the Supplemental Material [26], this valley selectivity is caused by the reflection from the bottom monolayer at the van der Waals heterointerface.

In order to study the dependence of the effect on the number of layers, we perform spatially resolved measurements over different flakes. The laser spot position on the heterostructure is controlled by a three-axis stage supporting

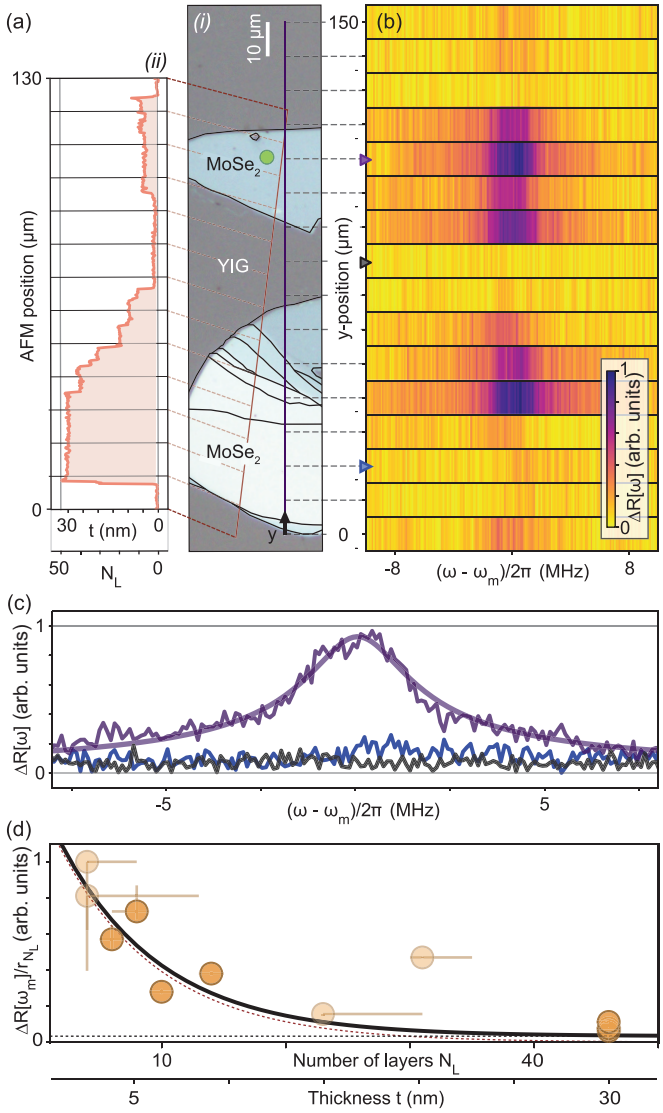

FIG. 3. Thickness dependence of the magneto-optical response. (a) Optical micrograph of the heterostructure under white light illumination (*i*) abutting a topography measurement along the dark orange line realized with an atomic force microscope (*ii*), where t is the calibrated thickness and N_L is the deduced number of $MoSe_2$ layers [26]. Black contours highlight change in optical contrast. A green circle marks the region investigated in the calibrated measurements in Fig. 4. The horizontal dashed lines along the y axis mark the successive positions of the laser spot center (waist radius: 2 μm). (b) Differential optical reflectance $\Delta R[\omega] = |R_+[\omega] - R_-[\omega]|$ around the magnon frequency as a function of the laser position on the sample. The spectra at positions $y = 80$ μm (black), $y = 20$ μm (blue), and $y = 110$ μm (purple) are shown in (c), corresponding respectively to bare YIG, a thick $MoSe_2$ flake ($N_L \sim 46$), and a few-layer $MoSe_2$ flake ($N_L \sim 8$). The purple translucent line is a Lorentzian fit ($\omega_m/2\pi = 5.58$ GHz). (d) Decay of the normalized differential optical reflectance with the $MoSe_2$ number of layers while driving magnons at $\omega_m/2\pi$. The solid thick line is a fit with a model of the fraction of light coming back from the very bottom layer (red dotted line) and a plateau (black dotted line). Data with large error bars in brown, marked as translucent, are not used for the fit [26]. Note that the point reported at $t \sim 20$ nm encompasses different terraces and cannot be normalized properly.

the optical microscope. An optical micrograph of the flakes under scrutiny is presented in Fig. 3(a)(*i*), accompanied by a topography measurement realized with an atomic force microscope shown in Fig. 3(a)(*ii*). We define the differential optical reflectance $\Delta R[\omega] = |R_+[\omega] - R_-[\omega]|$, with $R_\pm[\omega]$ the modulation signals of the reflection originating from $\sigma_\pm$ optical polarizations, such that their π-phase difference is highlighted. Figure 3(b) presents $\Delta R[\omega]$ along the vertical section shown in Fig. 3(a)(*i*). This measurement shows a strong modulation of the reflected light when the laser illuminates $MoSe_2$ flakes with less than ten layers.

Dynamic effects on thinner flakes are actually belittled as the measured signal is proportional to the static optical reflection coefficient r_{N_L}, with N_L the number of $MoSe_2$ layers [26]. To underline the dynamic response, we model the local reflectance and examine $\Delta R[\omega_m]/r_{N_L}$ [Fig. 3(d)]. The observed dynamic effects decay with the number of layers, in a fashion similar to the fraction of light coming from the very bottom layer [26]. This qualitatively indicates that the magnon-exciton coupling originates mainly from interfacial exchange interactions [28]. The tail at large N_L may be in part attributed to the long-range effect of the tenuous dipolar field created by the magnons. As the static reflection coefficient r_{N_L} and the portion of light coming back from the bottom layer, respectively, increases and decreases with an increasing number of $MoSe_2$ layers, there is an optimum number of layers giving the largest reflected optical intensity at the FMR frequency ($N_L \sim 6$ in our experimental conditions [26]).

Finally, in order to get additional insights into the microscopic origin of the interaction, we quantitatively determine the magnon-exciton coupling rate g. We perform calibrated measurements of the magnon-induced excitonic resonance shifts. The calibration procedure consists of comparing the optical reflection modulations induced by a known number of magnons n_{magnon} and those induced by a modulation of the laser frequency itself with a known modulation depth, without driving any magnons [26]. The number of magnons n_{magnon} in the concerned magnetostatic mode is determined through the analysis of the FMR absorption spectra [26].

The dynamical valley Zeeman shift, collectively enhanced by a factor of $\sqrt{n_{\text{magnon}}}$ [29], is $\Delta\Omega_s = g\sqrt{n_{\text{magnon}}}$ [26]. We measure calibrated exciton resonance shifts while ramping the microwave excitation power pumping the magnons. The coupling rate g is obtained by extrapolating the excitonic resonance shifts induced by a single magnon. The measurement presented in Fig. 4 is realized on an eight-layer flake. The calibrated magnon-exciton coupling strengths are $\hbar g_+ = (4.4 \pm 0.9) \times 10^{-15}$ eV and $\hbar g_- = (3.1 \pm 0.7) \times 10^{-15}$ eV for left- and right-handed circular polarizations (equivalently $g_\pm/2\pi \sim 1$ Hz). These similar g values reflect that the excitons in the valleys K and K' have the same sensitivity to the dynamic magnetic field, as it could be expected for a static magnetization in the plane of the film [14]. The small discrepancy between the two values does not seem substantial and is most likely due to systematic errors such as the quality of the polarizing cubes and electrical environment. The Zeeman shift induced by the effective magnetic field generated by a single magnon $B_{1\text{m}}$ can be written as $\hbar g = \Delta_\mu B_{1\text{m}}$, with Δ_μ the Zeeman shift of the exciton per unit magnetic field

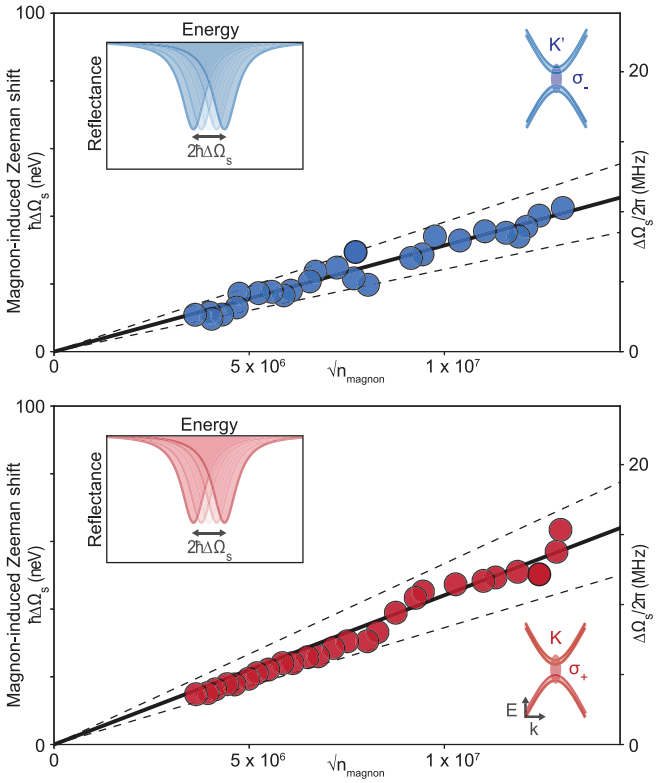

FIG. 4. Magnon-exciton coupling strength. Evolution of the magnon-induced valley Zeeman shift $\hbar\Delta\Omega_s$ with the number of magnons n_{magnon} for a few-layer flake [$N_L \sim 8$, marked by a circle in Fig. 3(a)] for σ_- and σ_+ optical polarization on the upper and lower panels, respectively. The thick solid lines correspond to linear fits, leading to magnon-exciton coupling strengths of $\hbar g_- = (3.1 \pm 0.7) \times 10^{-15}$ eV and $\hbar g_+ = (4.4 \pm 0.9) \times 10^{-15}$ eV for the K' and K valleys, respectively, exceeding the estimated value for a coupling originating purely from dipolar effects $\hbar g_{\text{D}} = 1.2 \times 10^{-17}$ eV, suggesting that exchange interactions are at play [26]. The inset sketches are exaggerated for the sake of clarity.

($\Delta_\mu = 0.12$ meV/T for $MoSe_2$ monolayers [8]). We evaluate the dipolar magnetic field produced by a single magnon, small but nonzero for a finite-size sample, as 0.1 pT and the resultant dipolar-originated magnon-exciton coupling strength as $\hbar g_{\text{D}} = 1.2 \times 10^{-17}$ eV ($g_D/2\pi \sim 3$ mHz [26]). This value constitutes an upper limit for the dipolar contribution to the effective magnon-exciton coupling strength. Finding magnon-exciton coupling rates $g \gg g_{\text{D}}$ adds another evidence that the exchange interaction at these van der Waals heterointerfaces is the dominant cause of the dynamical valley Zeeman effect we observe.

In conclusion, we have demonstrated qualitatively and quantitatively the magnon-exciton coupling at a heterointerface formed by an atomically thin semiconductor and a magnetic film by dynamic proximity effects. This hybrid system allows a control of the excitonic resonances at microwave frequencies at room temperature. Reducing the size of the magnetic film will confine the magnetic energy and enhance the magnetization oscillation amplitude per single magnon, leading to a stronger magnon-exciton coupling by 3–4 orders of magnitude [26]. By optimizing the sample preparation methods and improving the interface quality, the proximity coupling may be further increased. Our work initiates the investigation of dynamic magnetic proximity effects at van der Waals heterointerfaces [30–33] towards the dynamical local control of the excitons properties, through exotic spin textures for example [34], valley-dependent spin transport [35] and novel microwave-to-optics transducers [36–38], establishing multiple promising routes for interconnecting efficiently optics and spin physics.

This work is supported by JSPS KAKENHI (Grants No. 19K14626 and No. 19H05602) and by JST ERATO project (Grant No. JPMJER1601). We thank F. Fu, D. Lachance-Quirion, Y. Tabuchi, S. Daimon, T. Ideue, M. Ueda, L. Kaunitz, and S. Berciaud for fruitful interactions, and P. I. Sund for carefully reading the manuscript.

[1] A. K. Geim and I. V. Grigorieva, Van der Waals heterostructures, Nature (London) **499**, 419 (2013).

[2] D. Xiao, G. B. Liu, W. Feng, X. Xu, and W. Yao, Coupled Spin and Valley Physics in Monolayers of MoS_2 and Other Group-VI Dichalcogenides, Phys. Rev. Lett. **108**, 196802 (2012).

[3] G. Wang, A. Chernikov, M. M. Glazov, T. F. Heinz, X. Marie, T. Amand, and B. Urbaszek, Colloquium: Excitons in atomically thin transition metal dichalcogenides, Rev. Mod. Phys. **90**, 021001 (2018).

[4] K. F. Mak, D. Xiao, and J. Shan, Light-valley interactions in 2D semiconductors, Nat. Photonics **12**, 451 (2018).

[5] K. F. Mak and J. Shan, Photonics and optoelectronics of 2D semiconductor transition metal dichalcogenides, Nat. Photonics **10**, 216 (2016).

[6] N. Lundt, L. Dusanowski, E. Sedov, P. Stepanov, M. Glazov, S. Klembt, M. Klaas, J. Beierlein, Y. Qin, S. Tongay, M. Richard, A. Kavokin, S. Höfling, and C. Schneider, Optical valley Hall effect for highly valley-coherent exciton-polaritons in an atomically thin semiconductor, Nat. Nanotechnol. **14**, 770 (2019).

[7] E. Lorchat, L. López, C. Robert, D. Lagarde, G. Froehlicher, T. Taniguchi, K. Watanabe, X. Marie, and S. Berciaud, Filtering the photoluminescence spectra of atomically thin semiconductors with graphene, Nat. Nanotechnol. **15**, 283 (2020).

[8] Y. Li, J. Ludwig, T. Low, A. Chernikov, X. Cui, G. Arefe, Y. D. Kim, A. M. van der Zande, A. Rigosi, H. M. Hill, S. H. Kim, J. Hone, Z. Li, D. Smirnov, and T. F. Heinz, Valley Splitting and Polarization by the Zeeman Effect in Monolayer $MoSe_2$, Phys. Rev. Lett. **113**, 266804 (2014).

[9] G. Aivazian, Z. Gong, A. M. Jones, R.-L. Chu, J. Yan, D. G. Mandrus, C. Zhang, D. Cobden, W. Yao, and X. Xu, Magnetic control of valley pseudospin in monolayer WSe_2, Nat. Phys. **11**, 148 (2015).

[10] A. Srivastava, M. Sidler, A. Allain, D. Lembke, A. Kis, and A. Imamoglu, Valley Zeeman effect in elementary optical excitations of monolayer WSe_2, Nat. Phys. **11**, 141 (2015).

[11] C. Zhao, T. Norden, P. Zhang, P. Zhao, Y. Cheng, F. Sun, J. Parry, P. Taheri, J. Wang, Y. Yang, T. Scrace, K. Kang, S. Yang, G. Miao, R. Sabirianov, G. Kioseoglou, W. Huang, A. Petrou, and H. Zeng, Enhanced valley splitting in monolayer WSe_2 due to magnetic exchange field, Nat. Nanotechnol. **12**, 757 (2017).

[12] T. Norden, C. Zhao, P. Zhang, R. Sabirianov, A. Petrou, and H. Zeng, Giant valley splitting in monolayer WS_2 by magnetic proximity effect, Nat. Commun. **10**, 4163 (2019).

[13] J. Qi, X. Li, Q. Niu, and J. Feng, Giant and tunable valley degeneracy splitting in $MoTe_2$, Phys. Rev. B **92**, 121403(R) (2015).

[14] B. Scharf, G. Xu, A. Matos-Abiague, and I. Zutic, Magnetic Proximity Effects in Transition-Metal Dichalcogenides: Converting Excitons, Phys. Rev. Lett. **119**, 127403 (2017).

[15] D. Stancil and A. Prabhakar, *Spin Waves: Theory and Applications* (Springer, New York, 2009).

[16] Y. Kajiwara, K. Harii, S. Takahashi, J. Ohe, K. Uchida, M. Mizuguchi, H. Umezawa, H. Kawai, K. Ando, K. Takanashi, S. Maekawa, and E. Saitoh, Transmission of electrical signals by spin-wave interconversion in a magnetic insulator, Nature (London) **464**, 262 (2010).

[17] A. V. Chumak, V. Vasyuchka, A. Serga, and B. Hillebrands, Magnon spintronics, Nat. Phys. **11**, 453 (2015).

[18] Y. Tabuchi, S. Ishino, A. Noguchi, T. Ishikawa, R. Yamazaki, K. Usami, and Y. Nakamura, Coherent coupling between a ferromagnetic magnon and a superconducting qubit, Science **349**, 405 (2015).

[19] D. Lachance-Quirion, Y. Tabuchi, A. Gloppe, K. Usami, and Y. Nakamura, Hybrid quantum systems based on magnonics, Appl. Phys. Express **12**, 070101 (2019).

[20] A. A. Clerk, K. W. Lehnert, P. Bertet, J. R. Petta, and Y. Nakamura, Hybrid quantum systems with circuit quantum electrodynamics, Nat. Phys. **16**, 257 (2020).

[21] V. L. Korenev, M. Salewski, I. A. Akimov, V. F. Sapega, L. Langer, I. V. Kalitukha, J. Debus, R. I. Dzhioev, D. R. Yakovlev, D. Müller, C. Schröder, H. Hövel, G. Karczewski, M. Wiater, T. Wojtowicz, Y. G. Kusrayev, and M. Bayer, Long-range *p-d* exchange interaction in a ferromagnet-semiconductor hybrid structure, Nat. Phys. **12**, 85 (2016).

[22] S. Freeman and J. J. Hopfield, Exciton-Magnon Interaction in Magnetic Insulators, Phys. Rev. Lett. **21**, 910 (1968).

[23] R. S. Meltzer, M. Y. Chen, D. S. McClure, and M. Lowe-Pariseau, Exciton-Magnon Bound State in MnF_2 and the Exciton Dispersion in MnF_2 and $RbMnF_3$, Phys. Rev. Lett. **21**, 913 (1968).

[24] P. Němec, E. Rozkotová, N. Tesařová, F. Trojánek, E. De Ranieri, K. Olejník, J. Zemen, V. Novák, M. Cukr, P. Malý, and T. Jungwirth, Experimental observation of the optical spin transfer torque, Nat. Phys. **8**, 411 (2012).

[25] T. Dietl and H. Ohno, Dilute ferromagnetic semiconductors: Physics and spintronic structures, Rev. Mod. Phys. **86**, 187 (2014).

[26] See Supplemental Material at http://link.aps.org/supplemental/10.1103/PhysRevB.105.L121403 for details on the theoretical model, experimental determination of the magnon-exciton coupling strength, discussions on the estimate of the magnon-exciton coupling strength, and additional experimental methods and data. It includes Refs. [11–13,15,27,39–50].

[27] A. Arora, K. Nogajewski, M. Molas, M. Koperski, and M. Potemski, Exciton band structure in layered $MoSe_2$: From a monolayer to the bulk limit, Nanoscale **7**, 20769 (2015).

[28] I. Žutić, A. Matos-Abiague, B. Scharf, H. Dery, and K. Belashchenko, Proximitized materials, Mater. Today **22**, 85 (2019).

[29] R. H. Dicke, Coherence in spontaneous radiation processes, Phys. Rev. **93**, 99 (1954).

[30] S. Shi, S. Liang, Z. Zhu, K. Cai, S. Pollard, Y. Wang, J. Wang, Q. Wang, P. He, J. Yu, G. Eda, G. Liang, and H. Yang, All-electric magnetization switching and Dzyaloshinskii-Moriya interaction in WTe_2/ferromagnet heterostructures, Nat. Nanotechnol. **14**, 945 (2019).

[31] D. MacNeill, J. T. Hou, D. R. Klein, P. Zhang, P. Jarillo-Herrero, and L. Liu, Gigahertz Frequency Antiferromagnetic Resonance and Strong Magnon-Magnon Coupling in the Layered Crystal $CrCl_3$, Phys. Rev. Lett. **123**, 047204 (2019).

[32] L. Ciorciaro, M. Kroner, K. Watanabe, T. Taniguchi, and A. Imamoglu, Observation of Magnetic Proximity Effect Using Resonant Optical Spectroscopy of an Electrically Tunable $MoSe_2/CrBr_3$ Heterostructure, Phys. Rev. Lett. **124**, 197401 (2020).

[33] O. Johansen, A. Kamra, C. Ulloa, A. Brataas, and R. A. Duine, Magnon-Mediated Indirect Exciton Condensation through Antiferromagnetic Insulators, Phys. Rev. Lett. **123**, 167203 (2019).

[34] V. Sluka, T. Schneider, R. Gallardo, A. Kákay, M. Weigand, T. Warnatz, R. Mattheis, A. Roldán-Molina, P. Landeros, V. Tiberkevich, A. Slavin, G. Schütz, A. Erbe, A. Deac, J. Lindner, J. Raabe, J. Fassbender, and S. Wintz, Emission and propagation of 1D and 2D spin waves with nanoscale wavelengths in anisotropic spin textures, Nat. Nanotechnol. **14**, 328 (2019).

[35] Y. Ominato, J. Fujimoto, and M. Matsuo, Valley-Dependent Spin Transport in Monolayer Transition-Metal Dichalcogenides, Phys. Rev. Lett. **124**, 166803 (2020).

[36] R. Hisatomi, A. Osada, Y. Tabuchi, T. Ishikawa, A. Noguchi, R. Yamazaki, K. Usami, and Y. Nakamura, Bidirectional conversion between microwave and light via ferromagnetic magnons, Phys. Rev. B **93**, 174427 (2016).

[37] N. J. Lambert, A. Rueda, F. Sedlmeir, and H. G. L. Schwefel, Coherent conversion between microwave and optical photons: An overview of physical implementations, Adv. Quantum Technol. **3**, 1900077 (2020).

[38] N. Lauk, N. Sinclair, S. Barzanjeh, J. Covey, M. Saffman, M. Spiropulu, and C. Simon, Perspectives on quantum transduction, Quantum Sci. Technol. **5**, 020501 (2020).

[39] S. Zeytinoğlu, C. Roth, S. Huber, and A. Imamoglu, Atomically thin semiconductors as nonlinear mirrors, Phys. Rev. A **96**, 031801(R) (2017).

[40] G. Scuri, Y. Zhou, A. A. High, D. S. Wild, C. Shu, K. De Greve, L. A. Jauregui, T. Taniguchi, K. Watanabe, P. Kim, M. D. Lukin, and H. Park, Large Excitonic Reflectivity of Monolayer $MoSe_2$ Encapsulated in Hexagonal Boron Nitride, Phys. Rev. Lett. **120**, 037402 (2018).

[41] P. Back, S. Zeytinoglu, A. Ijaz, M. Kroner, and A. Imamoglu, Realization of an Electrically Tunable Narrow-Bandwidth Atomically Thin Mirror Using Monolayer $MoSe_2$, Phys. Rev. Lett. **120**, 037401 (2018).

[42] A. A. Clerk, M. H. Devoret, S. M. Girvin, F. Marquardt, and R. J. Schoelkopf, Introduction to quantum noise, measurement, and amplification, Rev. Mod. Phys. **82**, 1155 (2010).

[43] D. Walls and G. Milburn, *Quantum Optics* (Springer Science, Berlin, 2007).

[44] Y. Niu, S. Gonzalez-Abad, R. Frisenda, P. Marauhn, M. Drüppel, P. Gant, R. Schmidt, N. Taghavi, D. Barcons, A. Molina-Mendoza, S. De Vasconcellos, R. Bratschitsch, D. Perez De Lara, M. Rohlfing, and A. Castellanos-Gomez, Thickness-dependent differential reflectance spectra of monolayer and few-layer MoS_2, $MoSe_2$, WS_2 and WSe_2, Nanomaterials **8**, 725 (2018).

[45] T. Holstein and H. Primakoff, Field dependence of the intrinsic domain magnetization of a ferromagnet, Phys. Rev. **58**, 1098 (1940).

[46] M. Koperski, M. Molas, A. Arora, K. Nogajewski, M. Bartos, J. Wyzula, D. Vaclavkova, P. Kossacki, and M. Potemski, Orbital, spin and valley contributions to Zeeman splitting of excitonic resonances in $MoSe_2$, WSe_2 and WS_2 monolayers, 2D Mater. **6**, 015001 (2018).

[47] E. M. Purcell, *Electricity and Magnetism* (McGraw-Hill, Boston, 1985).

[48] M. B. Jungfleisch, V. Lauer, R. Neb, A. V. Chumak, and B. Hillebrands, Improvement of the yttrium iron garnet/platinum interface for spin pumping-based applications, Appl. Phys. Lett. **103**, 022411 (2013).

[49] W. Shi, J. Ye, Y. Zhang, R. Suzuki, M. Yoshida, J. Miyazaki, N. Inoue, Y. Saito, and Y. Iwasa, Superconductivity series in transition metal dichalcogenides by ionic gating, Sci. Rep. **5**, 12534 (2015).

[50] A. Castellanos-Gomez, M. Buscema, R. Molenaar, V. Singh, L. Janssen, H. van der Zant, and G. Steele, Deterministic transfer of two-dimensional materials by all-dry viscoelastic stamping, 2D Mater. **1**, 011002 (2014).